Yale-NUIST Center on Atmospheric Environment

Impact of aerosol shortwave radiative effect on entrainment of the atmospheric boundary layer

Cheng Liu

YNCenter Weekly Video Conference
2016.12.09

Outline

- **Introduction**
- **Model and method**
  - LES model
  - SBDART model
  - Configurations of LES
- **Results and discussions**
  - Vertical profiles of heat fluxes
  - Entrainment flux
  - Entrainment flux ratio
  - Heat budgets of EZ
  - Structures of EZ
- **Summary and conclusions**
- **On-going work**

Introduction

- The growth of the atmospheric boundary layer (ABL) is mainly driven by surface fluxes and by the entrainment.
- As compared to surface fluxes, entrainment is not well understood because of limited observations (*Huang et al., 2011*).
- Entrainment is the process by which more highly buoyant air from the free atmosphere is engulfed by the ABL air. It is a critical process regulating the exchange of momentum and scalars between ABL and the overlying free atmosphere.

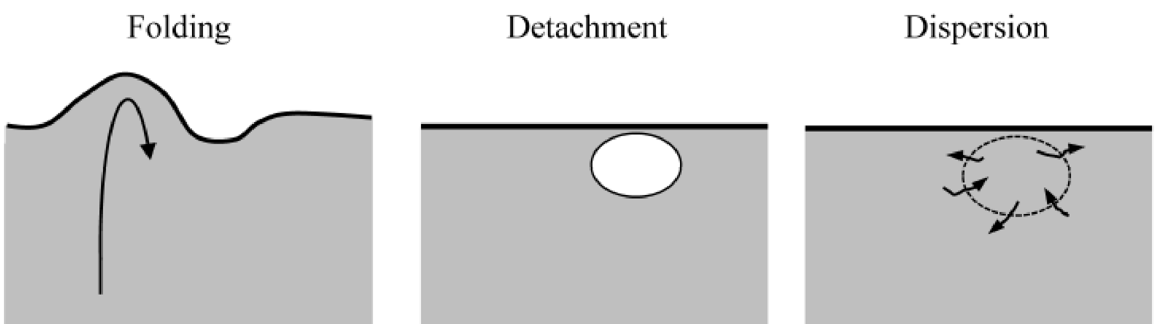

(**Source**: *Lee, fundamentals of Boundary-Layer Meteorology*)

Introduction (cont.)

- Previous observational and modelling studies were denoted to understand the parameterization of entrainment flux (*Lilly, 1968;Betts, 1974; Deardorff, 1979*), entrainment flux ratio (*Pina et al., 2003; Fedorovich et al., 2008, etc*) and entrainment budgets (*Sullivan et al., 1998, etc*). However, these results are gained from aerosol-free ABL.
- When aerosols present, they will modify surface fluxes and ABL's heat budget, eventually alter the evolution, structure and thermodynamics of *ABL(Yu et al., 2002; Barbaro et al., 2013*).
- In this study, we will extend previous studies to quantify the impact of aerosol shortwave radiative effects on the entrainment, especially for high aerosol loading and the existence of geostrophic winds.

Jump models

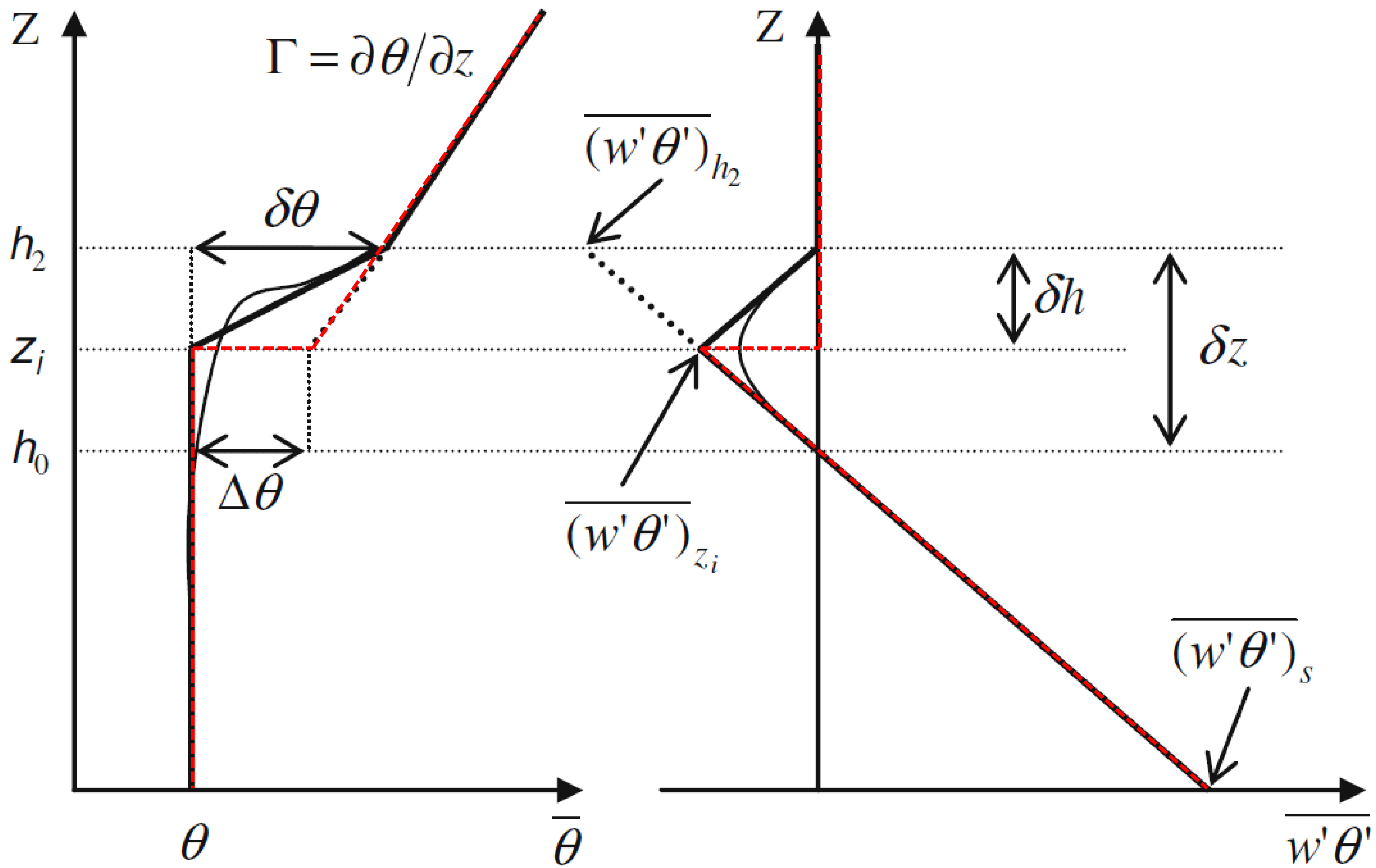

Fig.1 Sketch of zero-order (red dash line) and first-order (**black solid line**) jump model.
(**Source**: *Sun & Wang, 2008*)

The LES model

- The Large Eddy Simulation model employed in this study was originally developed by *Moeng (1984)*, and refined by *Sullivan (1996), Patton et al. (2005)* and Huang et al. (2008, 2009, and 2011).

- A radiation heating term (i.e. $\frac{1}{\rho c_p}\frac{\partial \overline{F}}{\partial z}$) is added to the potential temperature equation to assess the impact of aerosol radiative effect on the atmospheric boundary layer.

$$\frac{\partial \overline{\theta}}{\partial t} = -\overline{u}\frac{\partial \overline{\theta}}{\partial x} - \overline{v}\frac{\partial \overline{\theta}}{\partial y} - \overline{w}\frac{\partial \overline{\theta}}{\partial z} - \frac{\partial \tau_{\theta x}}{\partial x} - \frac{\partial \tau_{\theta y}}{\partial y} - \frac{\partial \tau_{\theta z}}{\partial z} + \frac{1}{\rho c_p}\frac{\partial \overline{F}}{\partial z}$$

The SBDART model

- The Santa Barbara DISORT(Discrete Ordinates Radiative Transfer) Atmospheric Radiative Transfer model (SBDART; *Ricchiazzi et al., 1998*) has been used widely to calculate aerosol radiative forcing and heating rate (*Kim et al., 2004; Tripathi et al., 2007; Gao et al., 2008; Kedia et al., 2010; Liu et al., 2012*).
- Model inputs: 1. the basic information, like longitude, latitude, date, time, wavelength, height, surface albedo, atmospheric conditions; 2. aerosol parameters, like AOD, single scattering albedo (SSA), and asymmetric factor (g).
- Model outputs: radiative flux density and heating rate at different layers.

Vertical profiles of heating rate

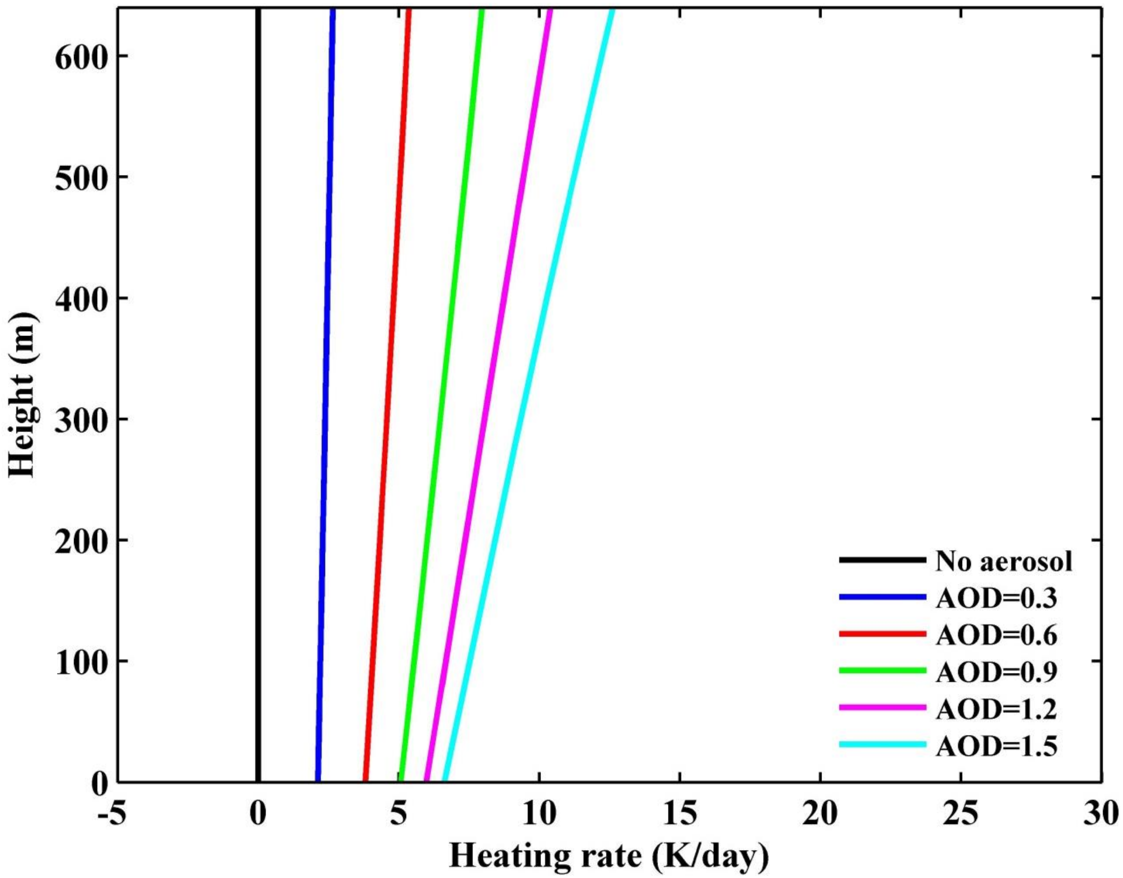

Aerosol is confined within boundary layer with uniform distribution, so the heating rate is zero above the boundary layer !

Fig.2 The vertical distribution of calculated heating rates with different AOD values (SSA=0.9, g=0.6) at time 12:00 on Jan 24th, 2015.

Configurations of the LES

Keep heat input consistent: $$HI = \overline{w'\theta_0'} + \int_0^{z_i} \overline{HR} dz$$

Table 1 Case design and input parameters.

Cases	u_g (m/s)	$\overline{w'\theta_0'}$ (K m/s)	HR*z_i (K m/s)	Initial z_i (m)
CTL	0, 5, 10, 15	0.1	0	640
A03	0, 5, 10, 15	0.082	0.018	640
A06	0, 5, 10, 15	0.066	0.034	640
A09	0, 5, 10, 15	0.052	0.048	640
A12	0, 5, 10, 15	0.039	0.061	640
A15	0, 5, 10, 15	0.029	0.071	640

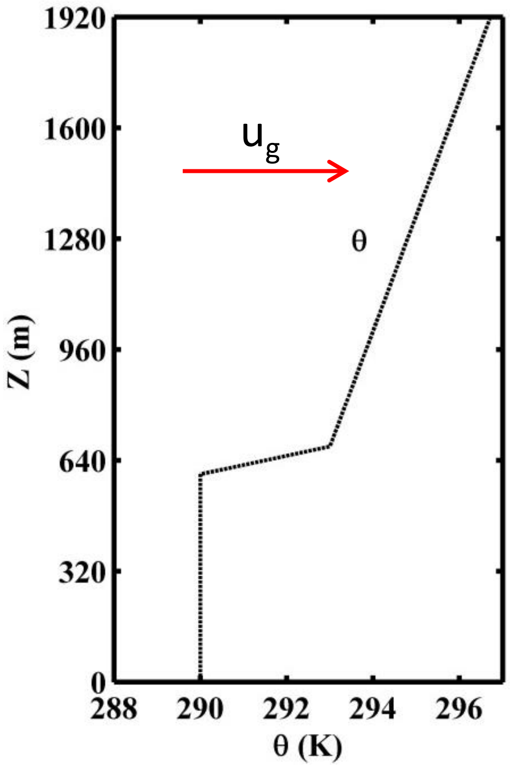

Fig.3 Initial profile of potential temperature

Results: Vertical profiles

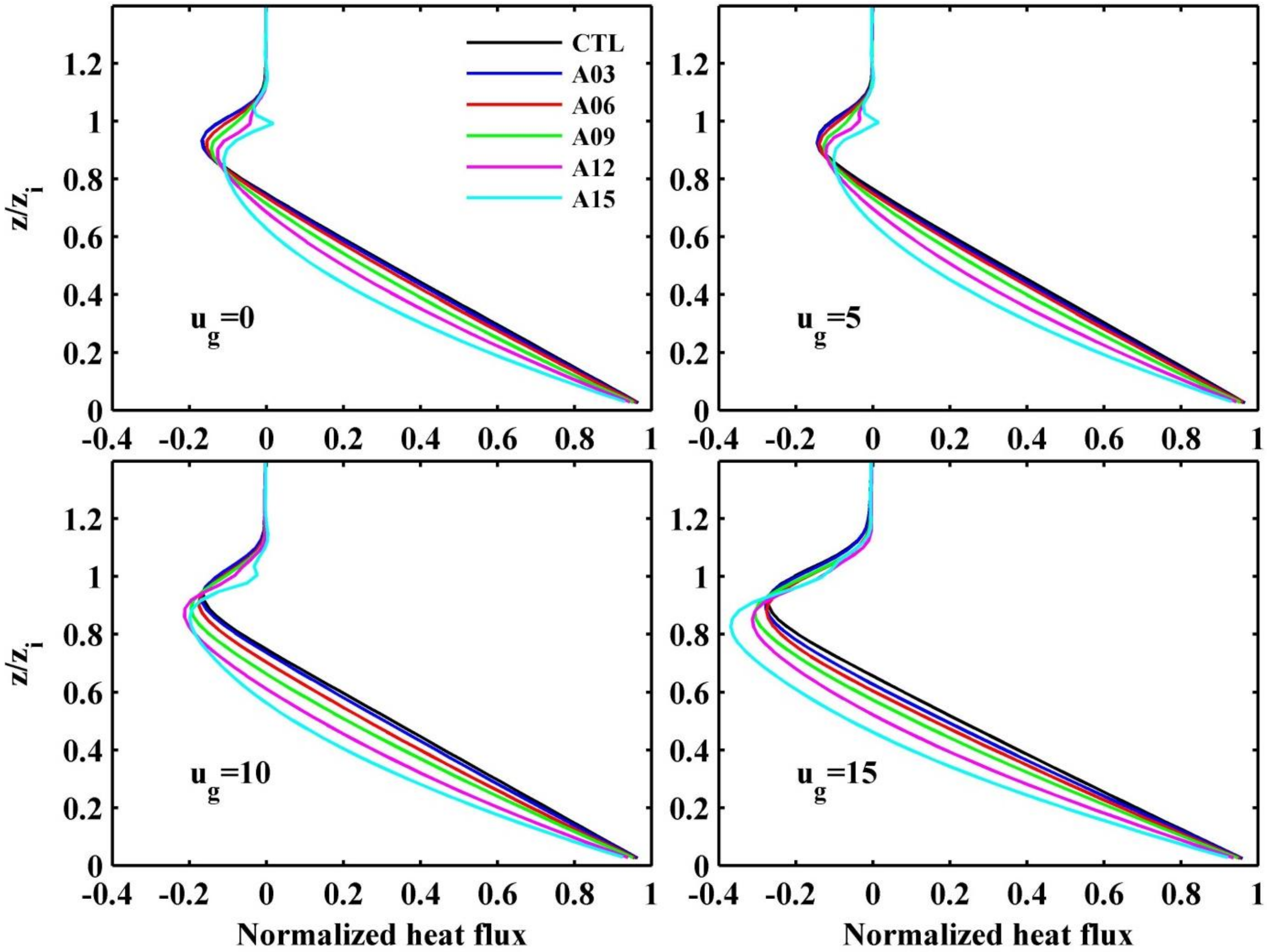

Fig.4 Vertical profile of normalized heat fluxes.

Results: entrainment fluxes

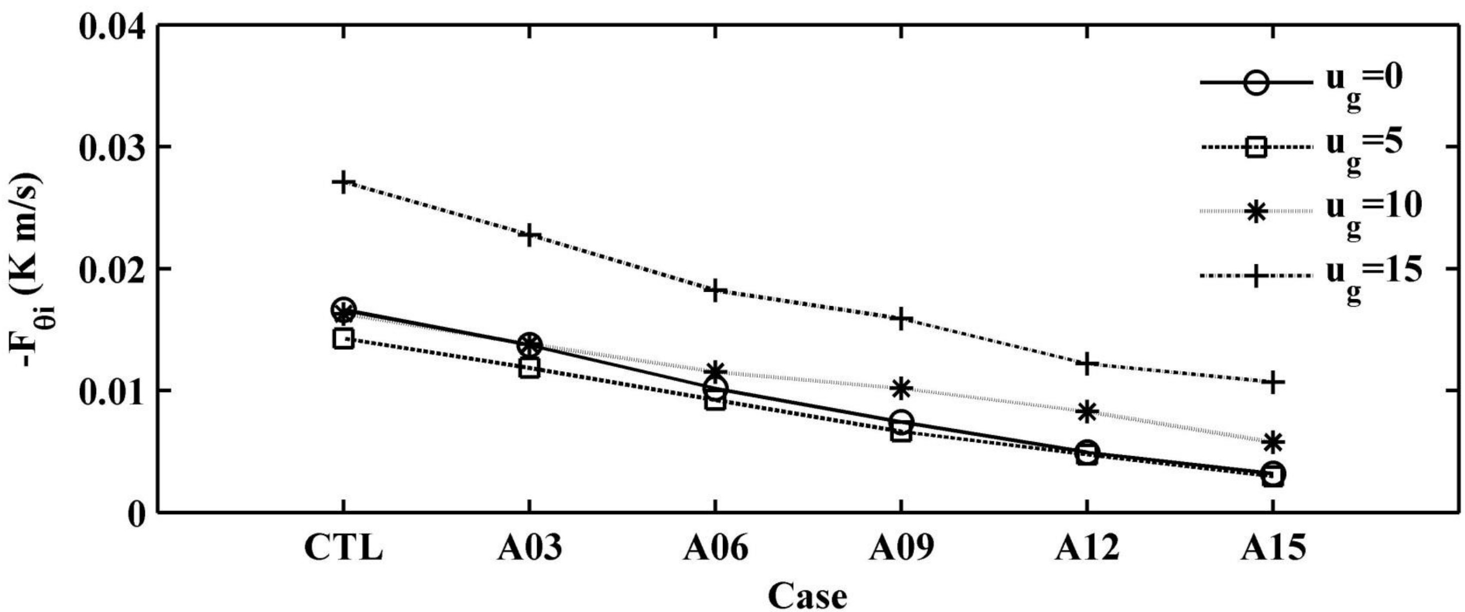

Fig.5 LES- resolved entrainment flux at z_i

u_g=0: Entrainment flux reduce 81% from CTL to A15.
u_g=15: Entrainment flux reduce 61% from CTL to A15.

Entrainment velocity and potential temperature jump

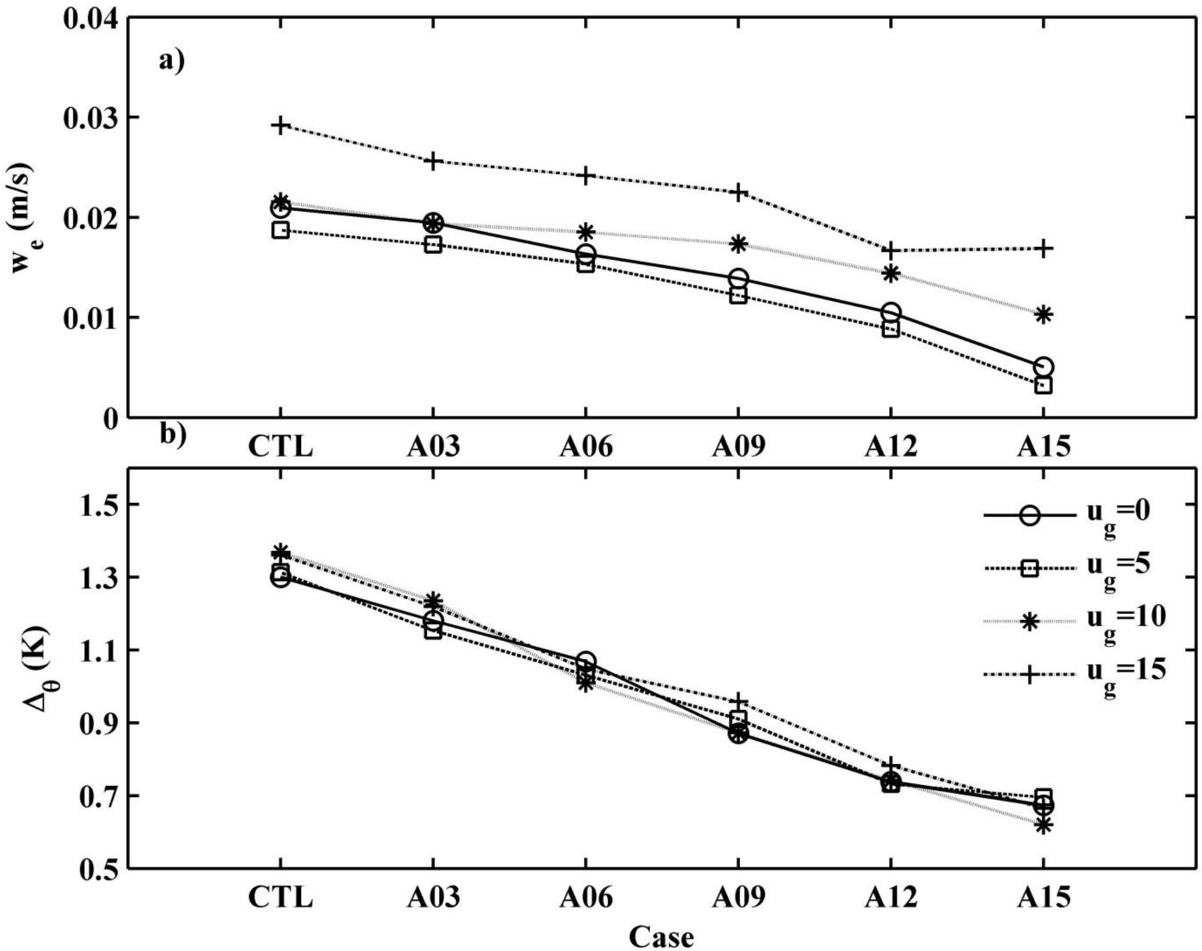

Fig.6 Entrainment velocity and potential temperature jump.

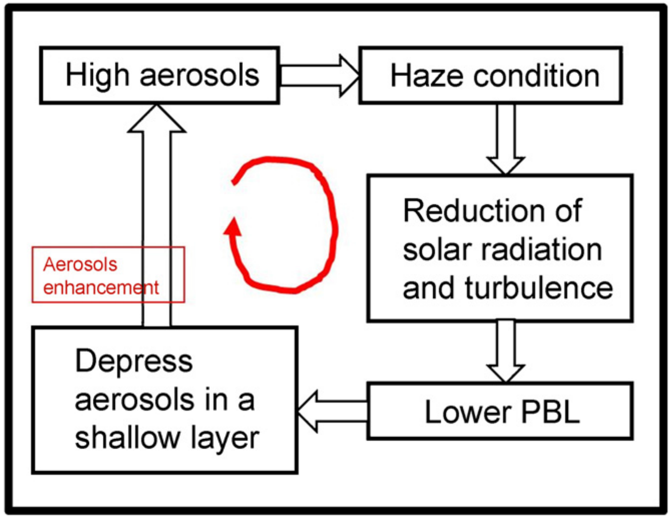

Source: *Quan et al., 2013*

Entrainment flux ratio

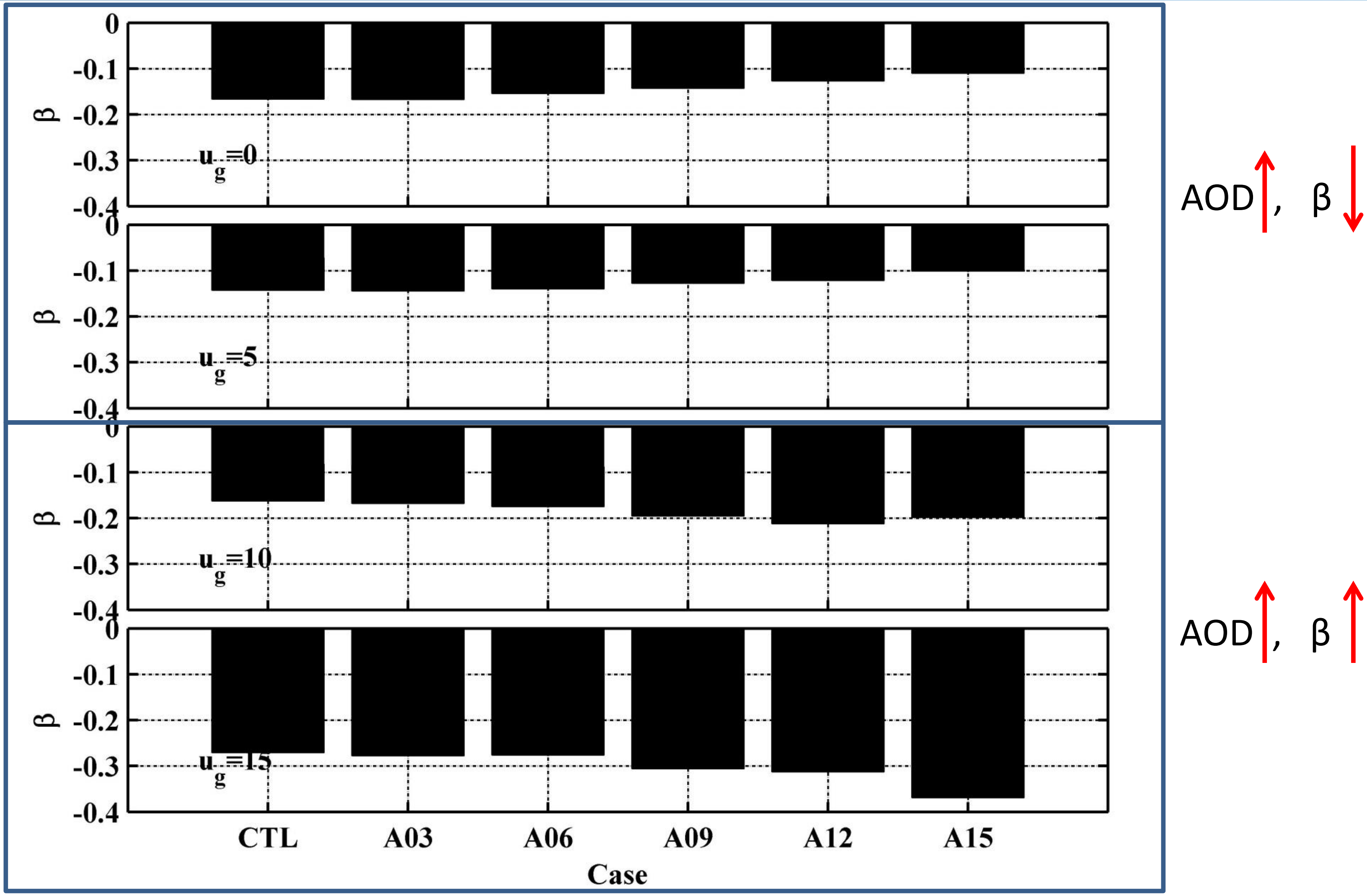

Fig.7 The ratio of entrainment heat flux to surface heat flux under different cases

Heat budgets of entrainment zone

$$w_e \delta\theta = -\overline{w'\theta'_{z_i}} + \delta z \frac{\partial \hat{\theta}}{\partial t} - \int_{z_i}^{z_1} \overline{HR} dz \qquad Ri = \alpha \delta\theta \frac{z_i}{w_*^2}$$

$$\frac{w_e}{w_*} = \frac{1}{Ri}(\beta_{w\theta} + \beta_{\delta z} - \beta_{HR}) \quad \text{where} \quad \beta_{w\theta} = -\overline{w'\theta'_{z_i}} / \overline{w'\theta'_0} \qquad \beta_{\delta z} = (\delta z \frac{\partial \hat{\theta}}{\partial t}) / \overline{w'\theta'_0} \qquad \beta_{HR} = \int_{z_i}^{z_1} \overline{HR} dz / \overline{w'\theta'_0}$$

(Betts, 1974; Sullivan et al., 1998; Barbaro et al., 2013)

Table 2. Heat budget at the entrainment zone under free convection.

case	$\beta_{w\theta}$ (%)	$\beta_{\delta z}$ (%)	β_{HR} (%)
CTL	0.166 (57.2)	0.125 (42.8)	-
A03	0.167 (44.1)	0.170 (44.6)	0.043 (11.3)
A06	0.154 (33.2)	0.210 (45.2)	0.100 (21.5)
A09	0.143 (20.8)	0.328 (47.8)	0.215 (31.4)
A12	0.126 (12.5)	0.487 (48.1)	0.400 (39.4)
A15	0.110 (7.6)	0.672 (46.4)	0.667 (46.0)

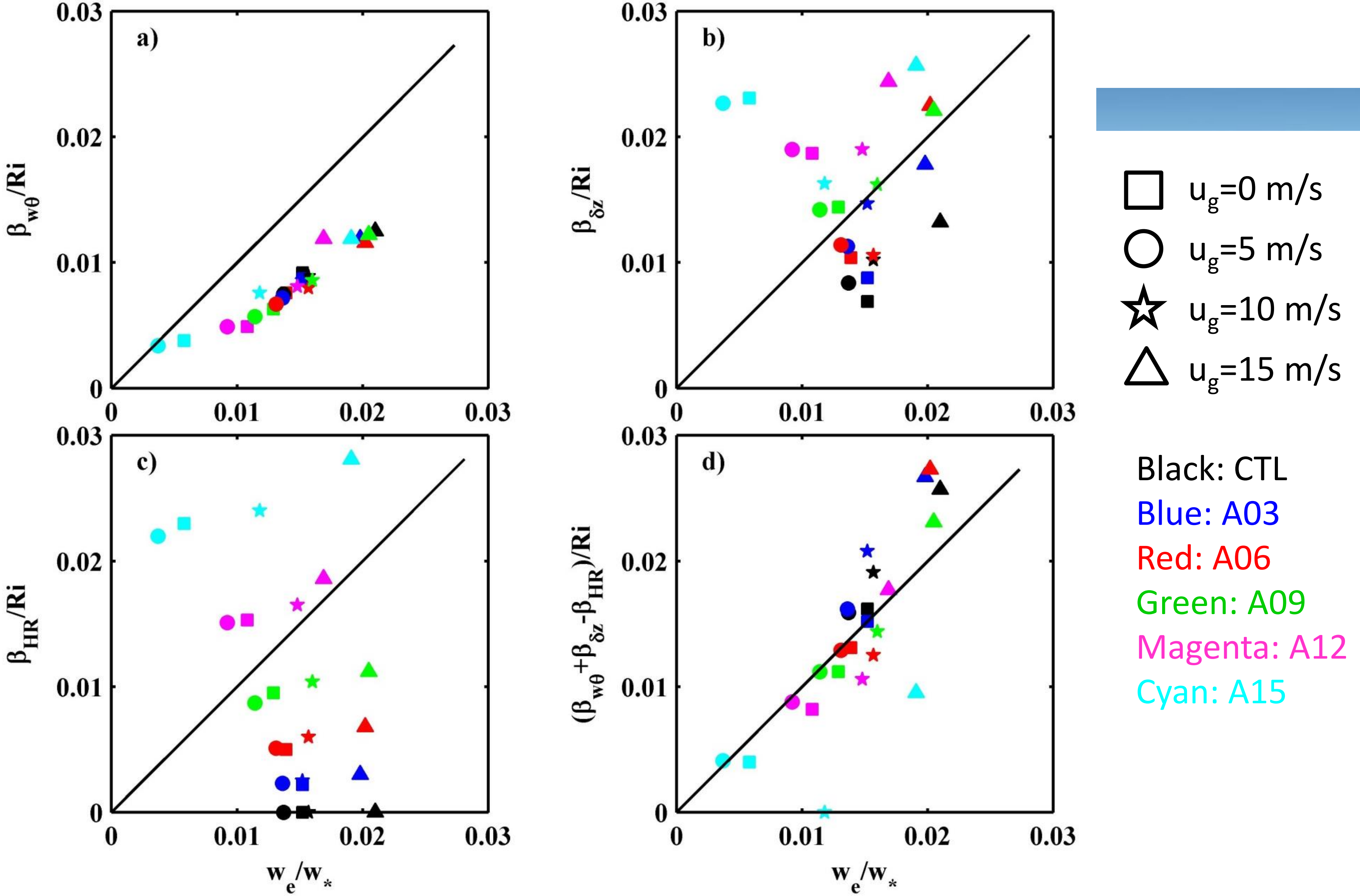

Fig.8 Comparison of first-order entrainment jump model and direct measurement of entrainment rate (w_e/w_*) .

Structures of EZ

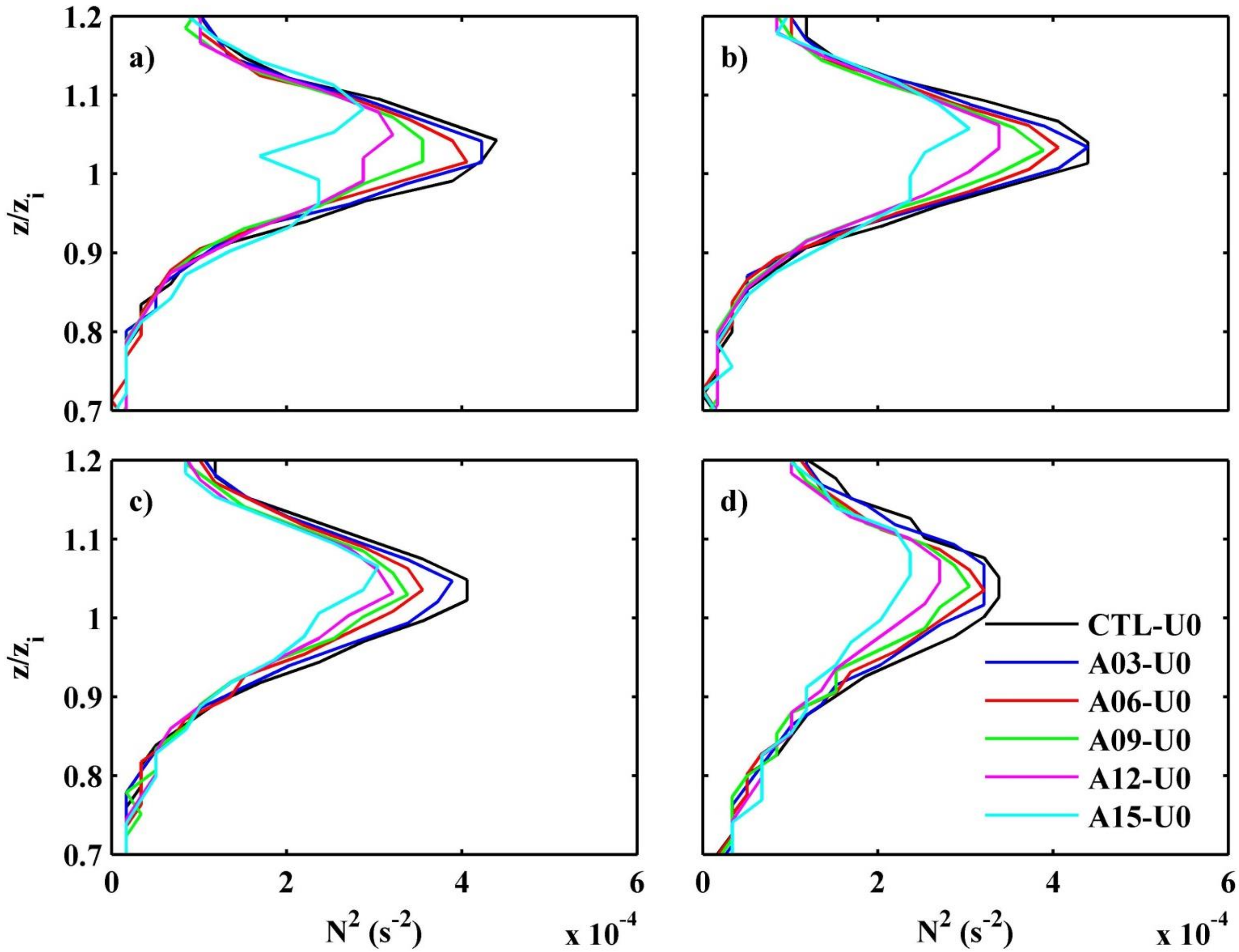

$$N^2 = \frac{g}{\theta_0}\frac{\partial\overline{\theta}}{\partial z}$$

More large N^2, more stably stratified atmosphere.

Fig.9 Vertical profiles of squared-Brunt-Vaisala frequency.

High-order statistics in EZ

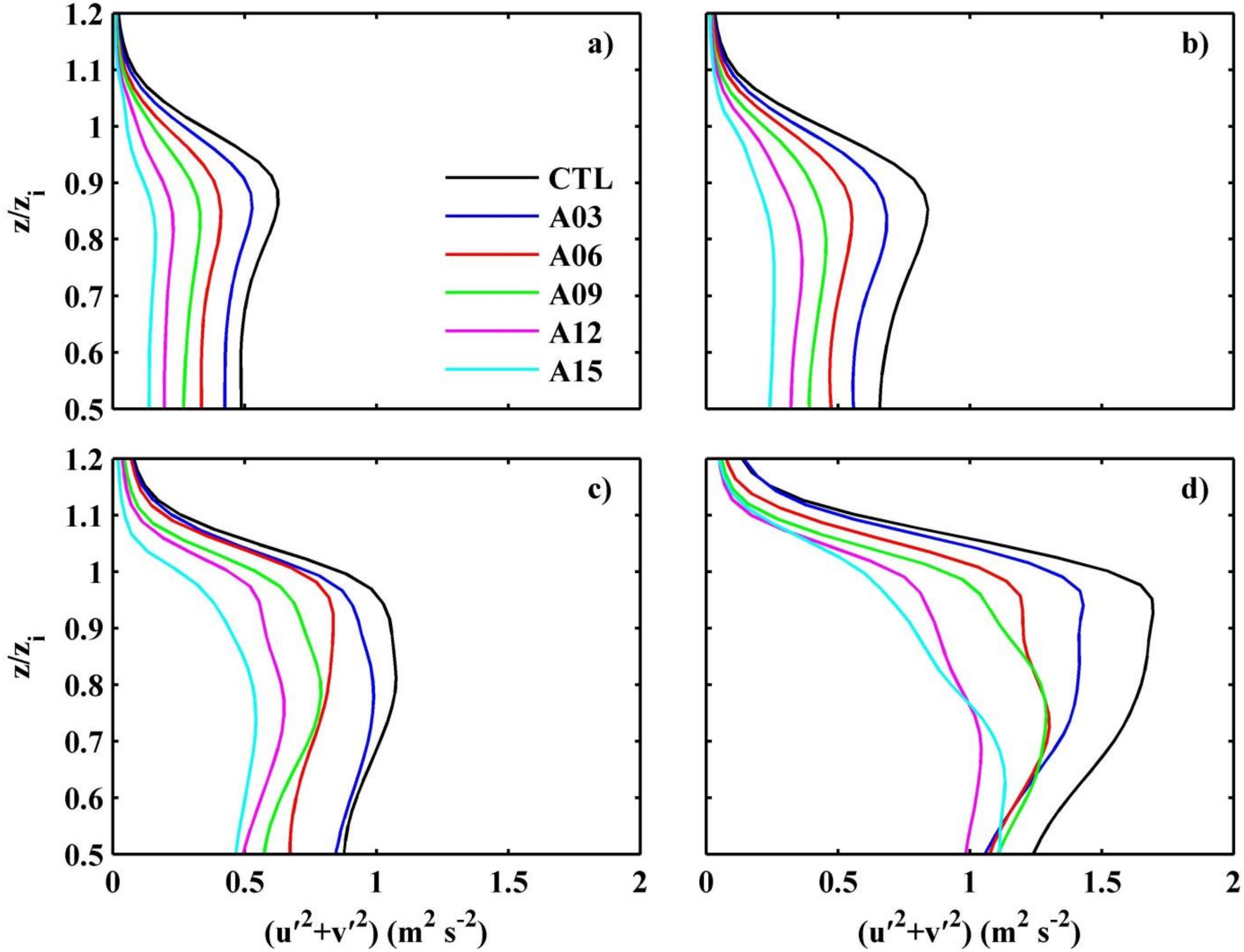

$$\frac{\overline{w'^2}}{\overline{u'^2+v'^2}}$$

Reduce from 0.31 for CTL to 0.21 for A15 under free convection, indicating 32% reduction for the conversion of vertical into horizontal motions.

Fig.10 Vertical profiles of horizontal velocity variance in the upper CBL.

High-order statistics in EZ (cont.)

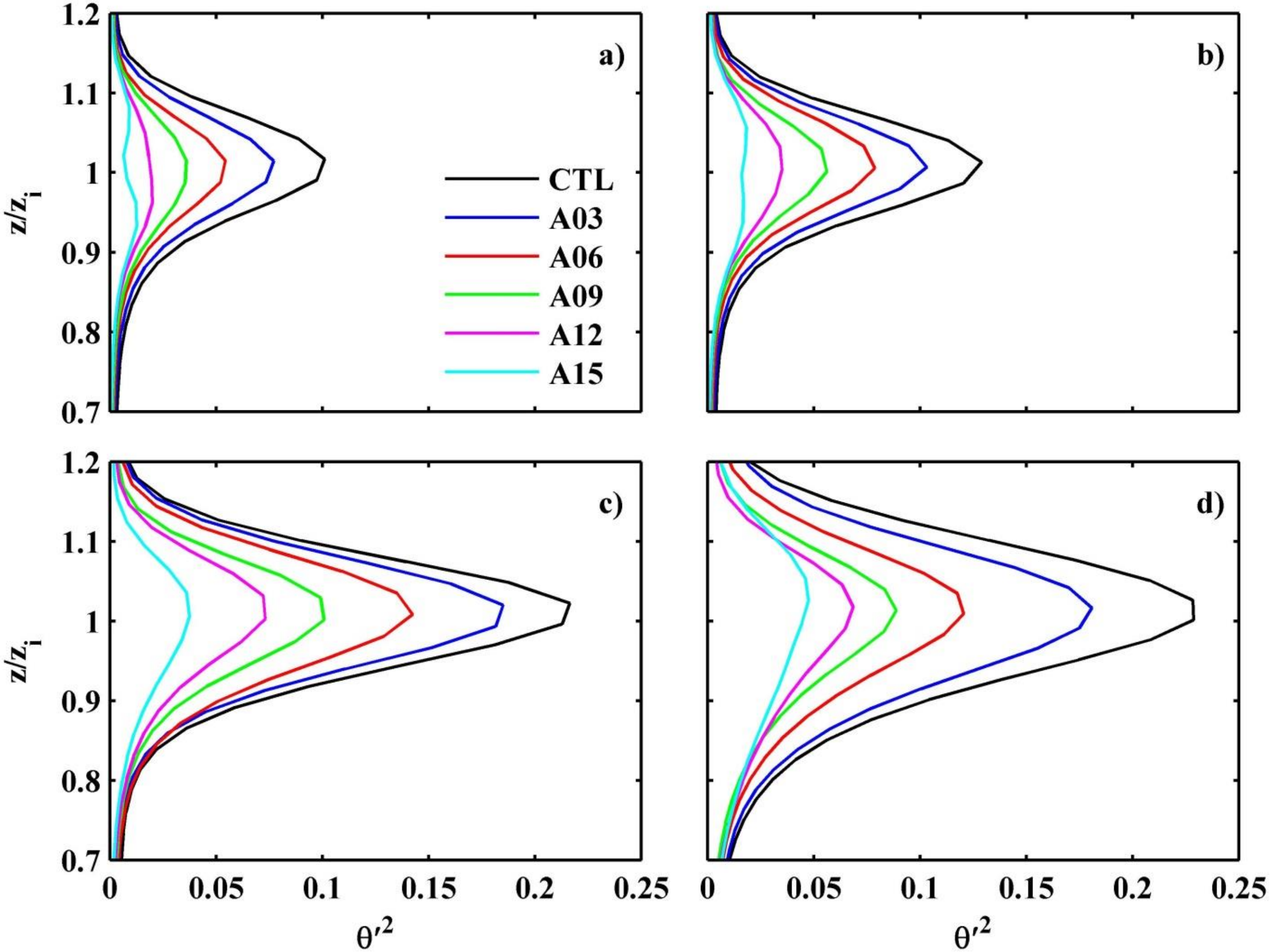

Fig.11 Vertical profiles of potential temperature variance in upper CBL.

Turbulence-organized structures

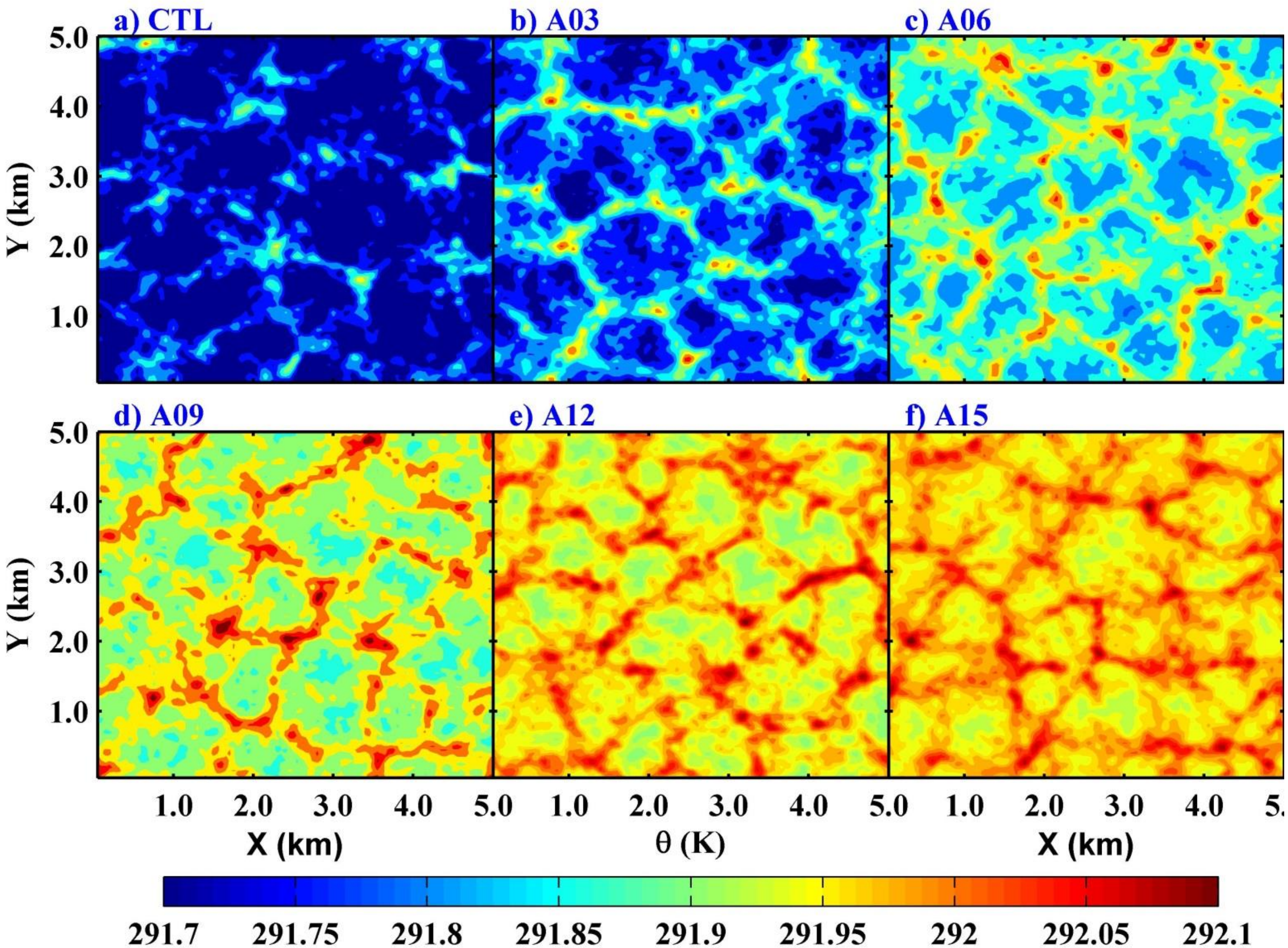

No impact on TOS feature!

Fig.12 Contours plots of hourly-averaged potential temperature field at 100m under free convection.

Cross-sections of vertical velocity

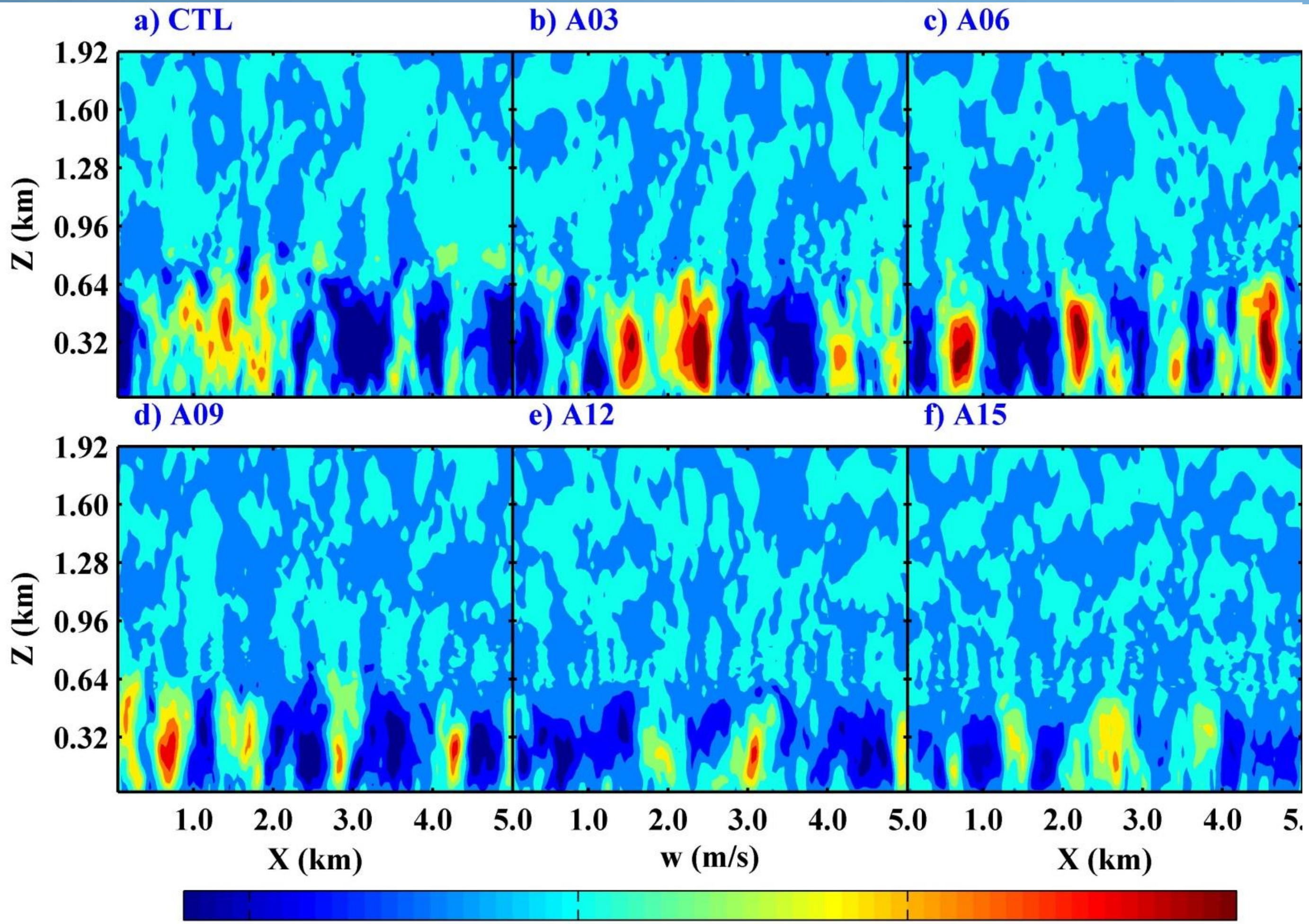

Fig.13 Contour plots of hourly-averaged vertical velocity field on an x-z plane under free convection.

Summary and conclusions

- Entrainment fluxes are decreased with increasing aerosol shortwave radiation absorption. Entrainment velocity and jump of potential temperature show similar variation trends.

- The entrainment flux ratios are decreased with increasing AOD under free convection and weak geostrophic wind (i.e. 5m/s). but the ratios show opposite trend with the AOD when geostrophic winds are greater than 10m/s.

- A first-order jump model is able to present the heat budget in the entrainment zone when aerosol radiative heating term is included.

- With impact of aerosol shortwave radiation effect, the jump of potential temperature was reduced and the EZ became less stable, Meanwhile, the horizontal velocity and potential temperature variances were decreased.

On-going work

- To add a aerosol mass conservation equation to the LES.
- To Include a LSM module for evaluating impact of aerosol radiation effect on diurnal variation of the atmospheric boundary layer.

Thank You !